Ultrasonics Sonochemistry 95 (2023) 106358

Contents lists available at ScienceDirect

Ultrasonics Sonochemistry

journal homepage: www.elsevier.com/locate/ultson

Tuned CuCr layered double hydroxide/carbon-based nanocomposites inducing sonophotocatalytic degradation of dimethyl phthalate

Tannaz Sadeghi Rad [a], Emine Sevval Yazici [a], Alireza Khataee [a,b,*], Erhan Gengec [c], Mehmet Kobya [a,d]

[a] Department of Environmental Engineering, Faculty of Engineering, Gebze Technical University, 41400 Gebze, Turkey
[b] Research Laboratory of Advanced Water and Wastewater Treatment Processes, Department of Applied Chemistry, Faculty of Chemistry, University of Tabriz, 51666−16471 Tabriz, Iran
[c] Department of Environmental Protection, University of Kocaeli, 41275 Izmit, Kocaeli, Turkey
[d] Department of Environmental Engineering, Kyrgyz-Turkish Manas University, 720038 Bishkek, Kyrgyzstan

ARTICLE INFO

Keywords:
Layered double hydroxide
Graphene
Advanced oxidation processes
Sonophotocatalysis
Dimethyl phthalate

ABSTRACT

This study is the first to explore the possibility of utilizing CuCr LDH decorated on reduced graphene oxide (rGO) and graphene oxide (GO) as sonophotocatalysts for the degradation of dimethyl phthalate (DMP). CuCr LDH and its nanocomposites were successfully fabricated and characterized. Scanning electron microscopy (SEM) along with high-resolution transmission electron microscope (HRTEM) both evidenced the formation of randomly oriented nanosheet structures of CuCr LDH coupled with thin and folded sheets of GO and rGO. The impact of diverse processes on the degradation efficiency of DMP in the presence of the so-prepared catalysts was compared. Benefiting from the low bandgap and high specific surface area, the as-obtained CuCr LDH/rGO represented outstanding catalytic activity (100 %) toward 15 mg L^{-1} of DMP within 30 min when subjected to light and ultrasonic irradiations simultaneously. Radical quenching experiments and visual spectrophotometry using an O-phenylenediamine revealed the crucial role of hydroxyl radicals compared to holes and superoxide radicals. Overall, outcomes disclosed that CuCr LDH/rGO is a stable and proper sonophotocatalyst for environmental remediation.

1. Introduction

Dimethyl phthalate (DMP, $C_{10}H_{10}O_4$) as a widespread plasticizer has been verified as a significant refractory contaminant owing to its high toxicity, bioaccumulation, endocrine disrupting impacts, and carcinogenesis [1]. DMP has been frequently determined in natural water sources at concentrations ranging from 0.1175 to 236000 g L^{-1}, which can be accumulated in the body and eventually imperil human and aquatic life [2,3]. As a consequence, it is imperative to determine the efficient treatment techniques for the disintegration of wastewater polluted with DMP [2,3]. The traditional treatment methods including adsorption and biodegradation can not be widely utilized according to the generation of secondary pollution sources, high cost, and the usage of hardly recycled catalysts [4]. Advanced oxidation processes (AOPs) have been immensely employed as simple, compatible, as well as promising treatment techniques to mineralize and eliminate a wide variety of pollutants, such as dyes, pesticides, pharmaceuticals, plasticizers, and heavy metals [5]. Among the AOPs, the photocatalytic process appears to be the promising route to disintegrate organic pollutants [6]. Nevertheless, photocatalysis still has some drawbacks including a high charge recombination rate and low mineralization of refractory contaminants. Hence, increasing interest has been paid to the application of sequential AOP hybrid techniques which can promote the mineralization of resistant compounds and decrement the overall operation cost [7]. Amongst, the sonophotocatalytic process is a kind of advanced integrated AOP involving a combination of photocatalysis and sonocatalysis [8]. This eco-friendly technique can employ ultrasound (US) and light irradiations as well as a proper heterogeneous catalyst to disintegrate wastewater effluents. Accordingly, substantial efforts have been devoted to amplifying the degradation efficiency (DE%) by the modification of reaction parameters and catalysts [9].

Among diverse heterogeneous catalysts applied to degrade organic contaminants in wastewater, increasing interest has been paid for two-dimensional LDHs. LDHs own a lamellar ionic structure along with the

* Corresponding author at: Department of Environmental Engineering, Faculty of Engineering, Gebze Technical University, 41400 Gebze, Turkey.
E-mail address: akhataee@gtu.edu.tr (A. Khataee).

https://doi.org/10.1016/j.ultsonch.2023.106358
Received 25 January 2023; Received in revised form 1 March 2023; Accepted 3 March 2023
Available online 6 March 2023

brucite-like layers made up of bivalent and trivalent cations [10]. The space between hydroxyl layers is filled by the intervening anions such as nitrate, sulfate, carbonate, etc. Moreover, the hydroxide ion in the LDH can form hydrogen bonds with the anions and water molecules. Owing to the weak interlayer bonding, LDHs have belonged immense properties [11]. Particularly, LDHs containing Cu are widely used in a variety of catalytic domains owing to their unique structural characteristics and the promising catalytic activity of the Cu atom. Moreover, Cu^{2+} served as the divalent cation to enhance the formation of defects while Cr^{3+} demonstrated high visible light absorption [12]. Based on the literature review, CuCr LDH owns a low bandgap that enables simple electron-hole separation under visible light [13]. However, poor mobility of the charge carriers and fast recombination of the generated electron-hole occur which is the major bottleneck that restricts the application of LDHs as photocatalysts [14]. On the other hand, the significant feature of LDHs is the plethora of combinations of various compounds that can be implemented in the LDH structure. As an instance, Huang et al. [15] utilized MgAl LDH/TiO_2 for the photocatalytic disintegration of DMP for 8 h. The obtained outcomes revealed that the accumulation of DMP onto the composites and the surface hydroxyl groups of the LDH provide a synergistic effect, increasing the rate of DMP photocatalytic degradation. Also, peroxymonosulfate activation in the presence of CoFe LDH/BC was investigated by Ye et al. [16]. The BC-CoFe LDH/PMS system generated more ROSs. As a consequence, 100% dimethyl phthalate degradation efficiency during 60 min was reached. In addition, carbon-based LDHs have garnered superb interest nowadays as photocatalysts with the aim of boosting the stability and efficacy of the LDHs. Amongst, graphene derivatives own exceptional electrical conductivity and stability as well as the existence of numerous oxygen-containing functional groups [17,18].

In the present study, the GO/rGO-based CuCr LDH nanocomposites have been synthesized by facile co-precipitation and hydrothermal routes, respectively. The structural properties of the fabricated nanomaterials are evaluated by HRTEM, SEM, X-ray diffraction (XRD), Brunauer-Emmett-Teller (BET), and Fourier transform infrared spectrometer (FTIR) analyses. With the aim of recognizing the best catalyst and treatment process for the degradation of DMP, the efficiency of sonophotocatalysis, photocatalysis, sonocatalysis, and adsorption in the presence of CuCr LDH, CuCr LDH/GO, and CuCr LDH/rGO are investigated. The impact of various operational parameters on the DE% of DMP is assessed for the optimized catalyst. Following that, the dominant reactive oxygen species (ROSs) that participated in the sonophotocatalysis are determined by using different inhibitors. To investigate the stability of the catalyst during sonophotocatalysis, the reusability tests along with XRD and FTIR analyses of the reused catalyst were conducted. Lastly, the generated by-products throughout the treatment procedure are monitored through the gas chromatography-mass spectrometry (GC–MS) technique.

2. Experimental section

2.1. Chemicals and characterizations

Chromium (III) nitrate nonahydrate, diethyl ether, ethanol, sodium hydroxide pellets, *para*-benzoquinone, N, O-Bis (trimethylsilyl) acetamide, copper (II) nitrate trihydrate, isopropanol, hydrogen peroxide (30 %), nitric acid, and formic acid were procured from Merck (Germany). Dimethyl phthalate, potassium peroxymonosulfate (PMS), and O-phenylenediamine were supplied by Sigma-Aldrich (USA). GO was provided by Nanografi nanotechnology AS Co. (Turkey). The description of characterization techniques was stated in the supplementary data (**Text S1**).

2.2. Preparation of the catalysts

For the synthesis of CuCr LDH, $Cr(NO_3)_3{\cdot}9H_2O$ (4.57 g) and $Cu(NO_3)_2{\cdot}3H_2O$ (4.83 g) were dissolved in 40 mL of distilled water. Afterward, the NaOH solution (1 mol L^{-1}) was inserted drop by drop into the prepared solution to achieve a pH of 6 in the nitrogen atmosphere. The suspension was mixed at room temperature for another 24 h. After washing several times with deionized water, the CuCr LDH was centrifuged and dried at 60 °C.

For the preparation of GO-based CuCr LDH nanocomposite, 80 mg of GO was ultrasonically dispersed in distilled water. Moreover, the pH of the solution containing $Cu(NO_3)_2{\cdot}3H_2O$ and $Cr(NO_3)_3{\cdot}9H_2O$ was enhanced to 5.5. The GO solution was mixed with the obtained mixture and stirred for 24 h. The formed CuCr LDH/GO nanocomposite was centrifuged and dried as described for pristine CuCr LDH.

The preparation of the CuCr LDH/rGO sample was initiated by dispersing 80 mg of GO ultrasonically. The pH of $Cr(NO_3)_3{\cdot}9H_2O$ and $Cu(NO_3)_2{\cdot}3H_2O$ solution was raised to 9 and mixed with the GO solution. The ultimate suspension was transmitted to an autoclave and heated (19 h, 110 °C). The resultant precipitate was washed and dried. The overall synthesis method is briefly presented in Fig. 1**a**.

2.3. Sonophotocatalytic tests

The DMP solution containing the specific amount of the prepared samples was located in an ultrasonic bath (Elmasonic P, Germany) and instantaneously exposed to light and US irradiation. The concentration of residual DMP was assessed by tracking the absorbance peaks with a UV–Vis spectrophotometer (SU-6100, Perkin Elmer, USA) at about 275 nm. In an attempt to recognize and quantify the hydroxyl radical, O-phenylenediamine was applied as a tracer. The method of hydroxyl radical quantification was properly discussed by Fang et. al [19].

3. Results and discussion

3.1. Characterizations of CuCr LDH, CuCr LDH/GO, and CuCr LDH/rGO

The XRD spectra of the CuCr LDH, CuCr LDH/GO, and CuCr LDH/rGO are displayed in Fig. 1**b**. The peaks located at 2θ values of 10°, 20°, 34°, and 61° attributed to the (003), (006), (009), and (110) planes (JCPDS 00–035-0965) [20]. Besides, the graphene-based CuCr LDH nanocomposites exhibit the same peaks. Furthermore, there are no evident GO and rGO diffraction peaks, attributing to the effective dispersion and exfoliation of GO and rGO nanosheets or overlapping the peaks of GO/rGO (at 10° and 20°, respectively) with the index peaks of CuCr LDH. Also, similar peaks were reported by Ziegenheim et al. [21] for CuCr LDH. Also, all samples present a series of well-developed uniformly spaced (00 l) Bragg's reflections revealing a hexagonal layered structure with R − 3 m rhombohedral symmetry. Additionally, an in-plane (110) peak and a wide hump at $2\theta = 60.4°$ and $2\theta = 34°$ are evident in the XRD patterns of all catalysts which are assigned to the development of in-plane hexagonal turbostratic structure [20]. All these findings provide strong evidence of the proper synthesis of CuCr LDH and its nanocomposites.

The main functional groups of the CuCr LDH, CuCr LDH/GO, and CuCr LDH/rGO were determined by the FTIR analysis (Fig. 1**c**). The peaks in the range of 400–1000 cm^{-1} are related to the M−O and M−OH vibrations (M: Cu^{2+} and Cr^{3+} cations). The intercalated water molecules and stretching O-H groups of CuCr LDH are responsible for the broad peak centered at approximately 3450 cm^{-1} [22]. Combining the CuCr LDH with GO and rGO caused an increase in the intensity of the O-H stretching band which is assigned to the hydroxyl functional groups that existed in the GO/rGO structures. Besides, the absorption band at about 1630 cm^{-1} is created by the bending vibration of the O-H groups of intercalated H_2O structures [23]. The absorption peak at the wavenumber of 1050 cm^{-1} may be allocated to the carbonate anions which originated from the atmospheric CO_2 [21]. Moreover, the strong and sharp absorption peak at 1376 cm^{-1} is referred to as the antisymmetric

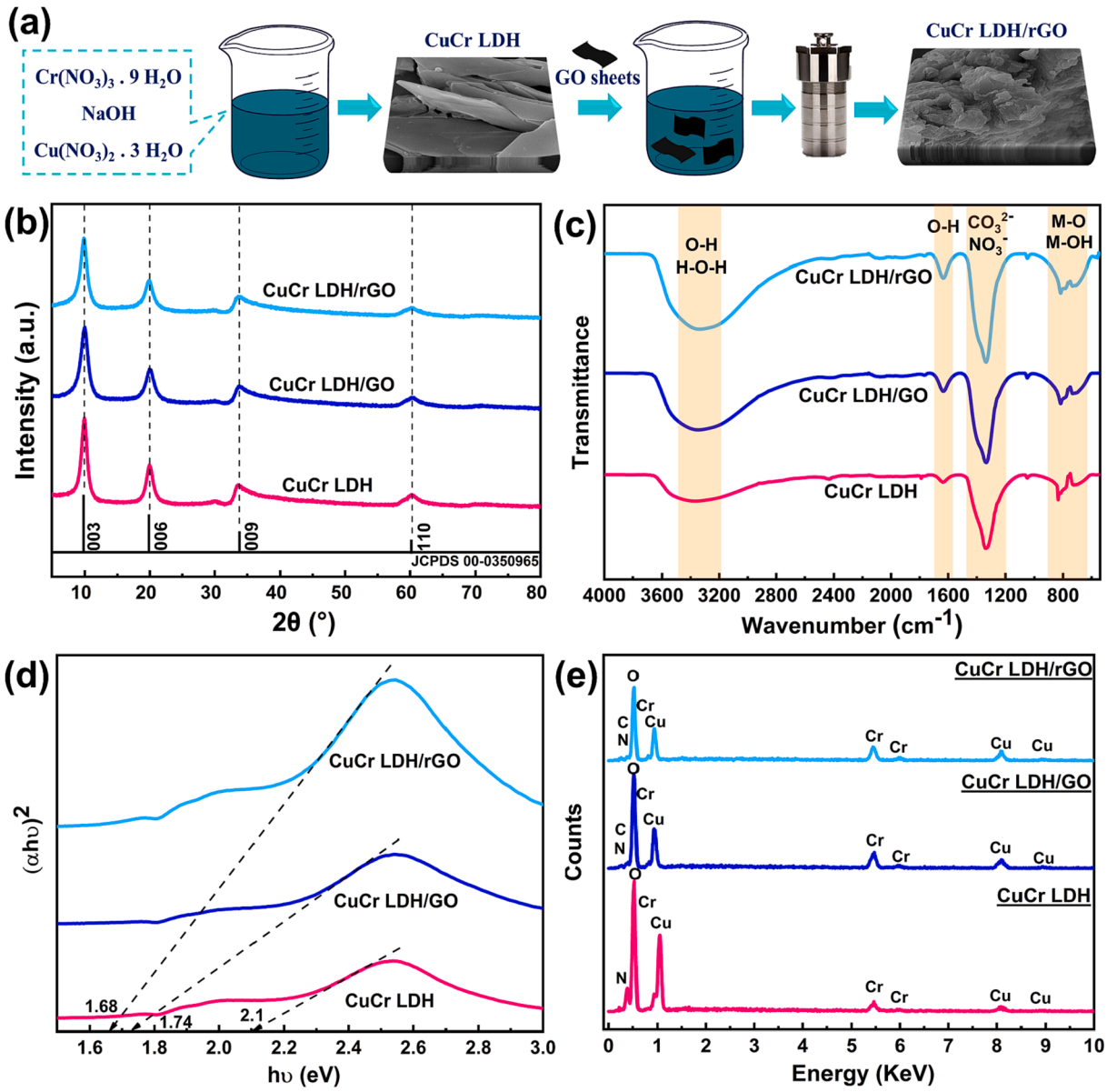

Fig. 1. (a) The schematic of the CuCr LDH/rGO's preparation, (b) the XRD patterns, (c) the FTIR spectra, (d) $(\alpha h\nu)^2$-hν curves, and (e) EDX of CuCr LDH, CuCr LDH/GO, and CuCr LDH/rGO.

stretching of intercalated NO_3^- [24].

The DRS analysis was applied to examine the optical properties and light responses of the as-prepared nanomaterials. Fig. 1**d** displays the $(\alpha h\upsilon)^2$-hυ curves of the CuCr LDH and its nanocomposites. To estimate the optical width of the bandgap, a tangent to the obtained curve was drawn. The computed bandgap energies of CuCr LDH, CuCr LDH/GO, and CuCr LDH/rGO were determined to be 2.1, 1.74, and 1.68 eV, respectively. It is believed that the narrower bandgaps facilitate the formation of photogenerated charges. Hence, this phenomenon improves the photocatalytic efficacy of the catalysts by producing high amounts of ROSs, which are beneficial for the decomposition of refractory contaminants. Consequently, CuCr LDH/rGO is expected to display high photocatalytic activity in comparison with CuCr LDH and CuCr LDH/GO. Also, in our previously published paper, a similar trend for bandgap was reported after the addition of carbon-based materials [25].

The elemental composition of the CuCr LDH and the carbonaceous nanocomposites has been estimated by EDX analysis and presented in Fig. 1**e**. The concurrent presence of copper, chromium, oxygen, and nitrogen elements in the chemical structure of CuCr LDH is affirmed. In the nanocomposite structures, carbon is also detected along with the other mentioned elements for the CuCr LDH. Thus, the efficacious synthesis of CuCr LDH, CuCr LDH/GO, and CuCr LDH/rGO is confirmed well by EDX analysis.

The N_2 adsorption–desorption isotherm was evaluated to find out the porosity of the samples. As can be seen from **Fig. S1**, the isotherms of all the nanomaterials could be categorized as type IV as a main characteristic of the mesoporous materials. However, differences in the hysteresis loops represent different pore shapes. According to the IUPAC classification, CuCr LDH and CuCr LDH/GO have H3-type hysteresis loops revealing the wedge-shaped pores created by the stacking of flaky particles [26]. On the other hand, CuCr LDH/rGO owns an H4-type hysteresis loop which can be implied that plate-like particles aggregated to form slit pores [27]. The specific surface area of 0.42, 1.64, and 8.3 $m^2 g^{-1}$ were obtained for CuCr LDH, CuCr LDH/GO, and CuCr LDH/rGO, respectively. CuCr LDH/rGO owns the highest specific surface area compared to CuCr LDH and CuCr LDH/GO.

The morphological features of the CuCr LDH, CuCr LDH/GO, and

CuCr LDH/rGO materials were characterized by SEM (Fig. 2**a-c**) and HRTEM (Fig. 2**d-f**). The SEM images of CuCr LDH represent thin nanosheets with apparent edges. Also, Patil et al. [20] observed unevenly shaped and randomly oriented nanosheets of CuCr LDH based on SEM analysis. By the addition of GO and rGO, the CuCr LDH layers are stacked among the thin nanosheets of GO and rGO. The folded layers of rGO nanosheets can be observed in Fig. 2**c**. As evidenced by SEM, the HRTEM micrographs disclosed randomly oriented nanosheet structures of CuCr LDH. Besides, thin layers of GO and rGO along with CuCr LDH structures are seen in Fig. 2**e and f**. Fig. 2**g** illustrated the dot-mapping

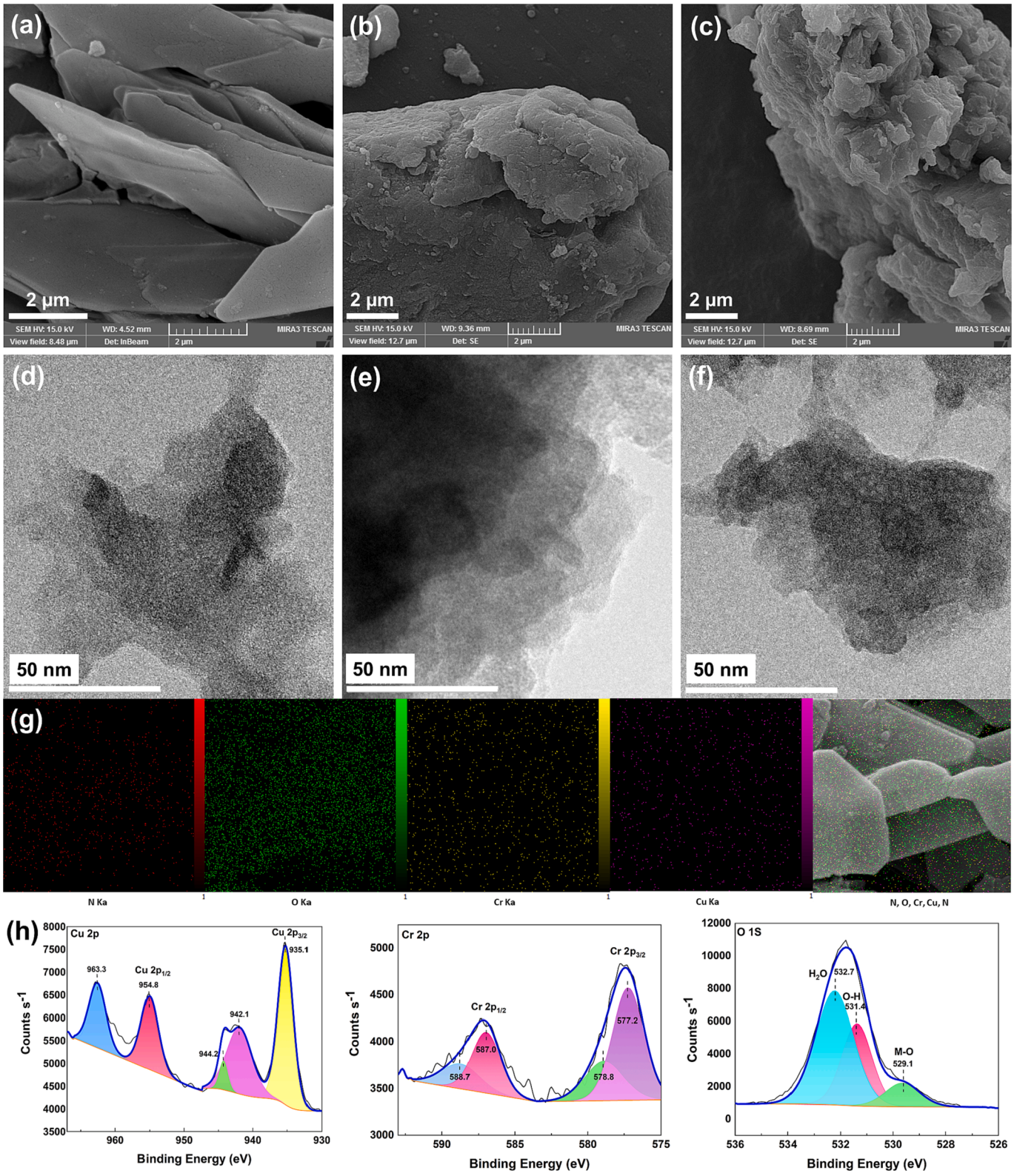

Fig. 2. (a, b, and c) The SEM, (d, e, and f) TEM images of CuCr LDH, CuCr LDH/GO, and CuCr LDH/rGO, (g) dot-mapping analysis of CuCr LDH, and (h) the XPS spectra of CuCr LDH: Cu 2p, Cr 2p, and O 1 s.

analysis of the CuCr LDH, affirming the existence of N, O, Cr, and Cu elements in the CuCr LDH structure. Besides, all the elements are distributed homogeneously along the sample structure.

XPS was used to assess the elemental state and composition of the prepared CuCr LDH (Fig. 2**h**). Cu 2p can be deconvoluted into 2 peaks; the Cu $2p_{1/2}$ peak appeared at 954.8, and the peak at 935.1 eV originated from the Cu $2p_{3/2}$. The other peaks of Cu 2p were localized at 942.1, 944.2, and 954.8 eV related to the Cu element in CuCr LDH, which is in the form of Cu^{2+}. The peaks of the Cr 2p spectrum localized at 577.2 and 587.0 eV display the contributions from the Cr $2p_{3/2}$ and Cr $2p_{1/2}$. This finding demonstrated that the Cr element corresponded to the Cr (III). The three peaks for O1s in the CuCr LDH spectrum are referred to H_2O, H-O, and O-M groups. Also, Zhang et al. [28] reported similar peak positions and states previously.

3.2. The catalytic degradation of DMP

3.2.1. The influence of various processes on the disintegration of DMP

The functions of CuCr LDH, CuCr LDH/GO, and CuCr LDH/rGO on DE% via diverse processes were conducted and depicted in Fig. 3. At the first step, the DE% of DMP were recognized under photolysis, sonolysis, and sonophotolysis. In the absence of a catalyst, low degradation efficiencies were achieved through the aforementioned processes relating to the recalcitrant nature of the DMP molecule. Even so, US irradiation can elevate the DE% owing to the growth and collapse of the aqueous bubbles which can generate hot spots for pyrolyzing water molecules. The formation of hydroxyl radicals through the pyrolyzation result in an increase in DE%. Therefore, the sonophotolysis process owns high efficacy in comparison with sonolysis and photolysis, as can be noticed from Fig. 3**a**.

During 30 min, the adsorption of the DMP molecules on CuCr LDH, CuCr LDH/GO, and CuCr LDH/rGO resulted in the DE% of about 19%, 20%, and 30%, respectively. In light of this, the adsorption process has a limited capacity to break down DMP molecules. However, the CuCr LDH/rGO owns higher DE% which could be attributed to its higher specific surface area compared to CuCr LDH and CuCr LDH/GO as examined via BET analysis. Besides, positively charged brucite-like layers of CuCr LDH in nanocomposite structure may interact electrostatically with the electron-rich aromatic ring or the oxygens of DMP molecule in the normal pH of DMP (pH = 8).

The photocatalytic behaviors of the so-synthesized samples were explored for 30 min (Fig. 3**a-c**). The CuCr LDH/rGO exhibits 40 % of DE % under photocatalysis. The higher photocatalytic activity of CuCr LDH/rGO can be attributed to low bandgap energy (1.68 eV) affirmed by DRS analysis. It was evidenced that a low bandgap can promote the transfer of electrons from the valence band to the conduction band. The generated electrons and holes can produce ROSs which can participate in the disintegration of DMP. Although, electrons and holes have a high affinity to recombine resulting in the alleviation of the DE%. To overcome this problem, GO and rGO can be intercalated as supports for LDHs which can serve as electron acceptors. Also, the addition of carbonaceous materials to the LDH structure can inhibit the agglomeration of the catalyst. Indeed, CuCr LDH/rGO and CuCr LDH/GO demonstrate high photocatalytic activity (40% and 37%, respectively) compared with CuCr LDH (29%).

The sonocatalytic process boosts the DE% by generating higher

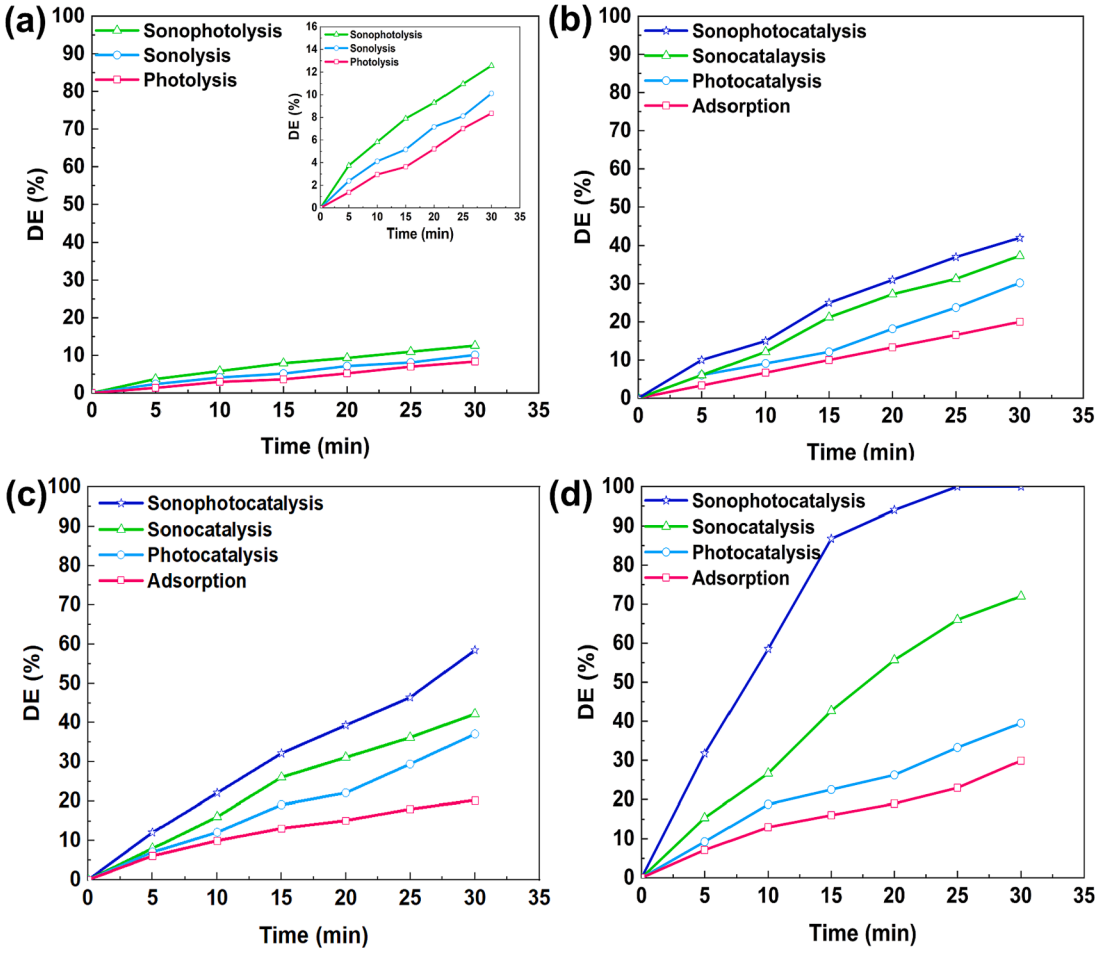

Fig. 3. The DE% of DMP via various processes (a) without catalyst; inset is the higher magnification of the image, (b) in the presence of CuCr LDH, (c) CuCr LDH/GO (d), and CuCr LDH/rGO ($[DMP]_0$ = 15 mg L^{-1}, [catalyst] = 0.75 g L^{-1}, pH = 8, US power = 150 W, and light intensity = 50 W).

amounts of ROSs. The DE% of DMP was promoted from 37.3% to 42.2%, and 72% by CuCr LDH, CuCr LDH/GO, and CuCr LDH/rGO, respectively. The higher specific area of CuCr LDH/rGO compared to CuCr LDH and CuCr LDH/GO can provide a suitable platform for the adsorption of DMP molecules, formation of diverse ROSs, and reactions among DMP molecules and ROSs. Also, Roso et al. [29] claimed that rGO-based nanocomposites had remarkable elimination efficiency due to the greater interaction of rGO with the photocatalyst and reduced mass-transfer restrictions. What's more, US irradiation is able to produce electron-hole pairs based on the sonoluminescence process exceeding the amounts of ROSs. Enormous bubbles were formed when solutions were subjected to severe ultrasonic irradiation. Under the cyclical ultrasonic vibration, these bubbles expanded, shrank, and eventually burst apart, causing hammering action on the solid–liquid interface. Besides, US waves can promote the DE% through scrubbing the catalyst surface, increment of mass transfer among the solution-CuCr LDH/rGO surface, and prevention of catalyst agglomeration.

As it can be monitored from Fig. 3**a-c**, the DE% boosted from 42% to 58.5% and 100% within 30 min in the presence of CuCr LDH, CuCr LDH/GO, and CuCr LDH/rGO, respectively. Furthermore, the synergy factor values were computed as 1.3, 2, and 25.5 in the presence of CuCr LDH, CuCr LDH/GO, and CuCr LDH/rGO based on the $\text{Synergy factor} = \frac{k_{app(Catalyst+Light+US)}}{k_{app(Catalyst)} + k_{app(Light)} + k_{app(US)}}$ equation, in which $k_{app(Catalyst+Light+US)}$, $k_{app(catalyst)}$, $k_{app(Light)}$, and $k_{app(US)}$ are the sonophotocatalysis, adsorption, photolysis, and sonolysis rate constants respectively. Eventually, CuCr LDH/rGO was chosen as an appropriate catalyst for the degradation of DMP under sonophotocatalysis. Additionally, the degradation turnover (dTON) value as a facile way to judge the catalytic degradation systems was estimated according to the $\text{dTON} = \frac{n_0 - n}{t \times C}$ in which n_0, n, t, and C display initial and ultimate moles of DMP (μmol), time (h), and catalyst amount (g), respectively [30]. 88.6, 120.6, and 205.9 μmol h^{-1} g^{-1} were calculated for CuCr LDH, CuCr LDH/GO, and CuCr LDH/rGO, respectively. Moreover, the efficiency of sonophotocatalysis can be computed in terms of the electrical energy per order (EEO) through the methodology presented in the literature [31]. EEO was computed by the $\text{EEO} = \frac{t \times P}{V \times \log\left(\frac{C_i}{C_f}\right)}$ equation in which V, t, P, C_f, and C_i are the volume of the DMP solution, the time of sonophotocatalysis, the sum of light and US powers, and the final and initial concentrations of DMP. The EEO value of 543.47 $kWhm^{-3}$ $order^{-1}$ was obtained for the decomposition of DMP through the sonophotocatalysis in the presence of CuCr LDH/rGO. An organized glimpse of data for the EEO values of the sonophotocatalytic process is illustrated in Table 1. It can be acknowledged that the present treatment technique owns reasonable EEO which could be considered a cost-effective route for the degradation of refractory organic contaminants.

3.2.2. The evaluation of operational parameters

The catalyst dosage is a key factor in the catalytic degradation processes which affects the economic treatment of refractory contaminants. Fig. 4**a** explains that the degradation extent of DMP boosts with an increase in catalyst dosage in the range of 0.5–1 g L^{-1}. This can be mainly related to the increment of the CuCr LDH/rGO active sites expediting the involved reactions to form ROSs, which are in charge of attacking pollutant molecules [34]. Notwithstanding, enhancing the catalyst dosage from 1 to 1.5 g L^{-1} resulted in reducing the DE% from 100 % to 95 % within 25 min. This can be owed to the aggregation of catalyst particles in the solution which not only hinders the energy (US and light) conduction to the catalyst's surface but also restricts the active sites of the catalyst to generate ROSs. Eventually, as the DE% of DMP in the presence of 0.75 and 1 g L^{-1} is the same (100 % during 25 min), 0.75 g L^{-1} was preferred as the suitable catalyst dosage from the economic point of view.

The influence of DMP initial concentration (10–30 mg L^{-1}) on the decomposition efficiency was pursued. As demonstrated in Fig. 4**b**, the DE% decremented from 100% to 48.2% as the initial concentration of DMP enhanced from 10 to 30 mg L^{-1}. This may be caused by the inadequate quantity of hydroxyl radicals in the reaction media despite the fact that the number of DMP molecules raises substantially. Thus, the generated hydroxyl radicals are constrained to attack the DMP molecules. Besides, the active sites of the CuCr LDH/rGO are conquered as a result of increased DMP concentration, which impedes heat and energy absorption [14]. A similar trend was reported previously by Oladipo et al. [35].

Table 1
Comparing the reported EEO values during sonophotocatalysis under different operational parameters.

Catalyst	Reaction condition	DE (%)	EEO ($kWhm^{-3}$ $order^{-1}$)	Refs.
TiO_2	[Ofloxacin] = 20 mg L^{-1}, [Catalyst] = 0.4 g L^{-1}, US frequency = 40 kHz, UV power = 125 W, and time = 120 min	88.1	2504.1	[31]
ZnO	[Ofloxacin] = 20 mg L^{-1}, [Catalyst] = 0.4 g L^{-1}, US frequency = 40 kHz, UV power = 125 W, and time = 120 min	94.2	2071.2	[31]
Bi_2MoO_6/$FeVO_4$	[Ciprofloxacin] = 10 mg L^{-1}, [Catalyst] = 0.5 g L^{-1}, [H_2O_2] = 20 mmol L^{-1}, Xenon power = 500 W, US power = 50 W, and time = 200 min	93.43	697.71	[32]
TiO_2	[2,4-dichlorophenoxyacetic acid] = 50 mg L^{-1}, [Catalyst] = 1 g L^{-1}, [H_2O_2] = 250 mg L^{-1}, UV power = 36 W, US power = 120 W, and time = 360 min	82.24	7797	[33]
CuCr LDH/rGO	[DMP] = 15 mg L^{-1}, [Catalyst] = 0.75 g L^{-1}, US power = 150 W, visible light power = 50 W, and time = 30 min	100	543.47	Present study

The effect of light intensity on the sonophotocatalytic degradation of DMP can be monitored in Fig. 4**c**. As the light intensity was increased from 30 to 50 W, the sonophotocatalytic activity was boosted from 96 to 100%. Remarkably, as light intensity raise, more photons are emitted which are responsible for activating photocatalysts, resulting in the generation of more e^- h^+ pairs and speeding up the degradation. At higher light intensities, a surplus of photons may not participate in the sonophotocatalytic reactions, which was confirmed by Askari et al. [36].

The amount of available cavitation bubbles can differ considerably based on the quantity of US power employed. Fig. 4**d** portrays the impact of ultrasonic power on the DE%. All the applied ultrasonic powers can reach the DE% of 100% during 25 min. However, the rate of the treatment process was boosted by increasing the amount of ultrasonic power. As ultrasonic power improves, not only the energy of cavitation is boosted, but also the cavitation threshold is reduced. Consequently, more cavitation microbubbles are yielded and thus more ROSs are generated [37]. Another possible explanation can be related to the high turbulence of the solution at high US power resulting in the mass transfer rate improvement of the DMP molecules from the aquatic medium to the CuCr LDH/rGO surface. Moreover, according to the cleansing characteristic of ultrasonic irradiations, the CuCr LDH/rGO's active sites are more available for reactions in high ultrasonic powers. Similar results were also obtained in our previously-published paper [14].

Since pH has a notable impact on the surface charge of the catalyst along with the solute pollutant molecules' state, the sonophotocatalytic efficacy of CuCr LDH/rGO was examined in the range of 4–12. Fig. 4**e**

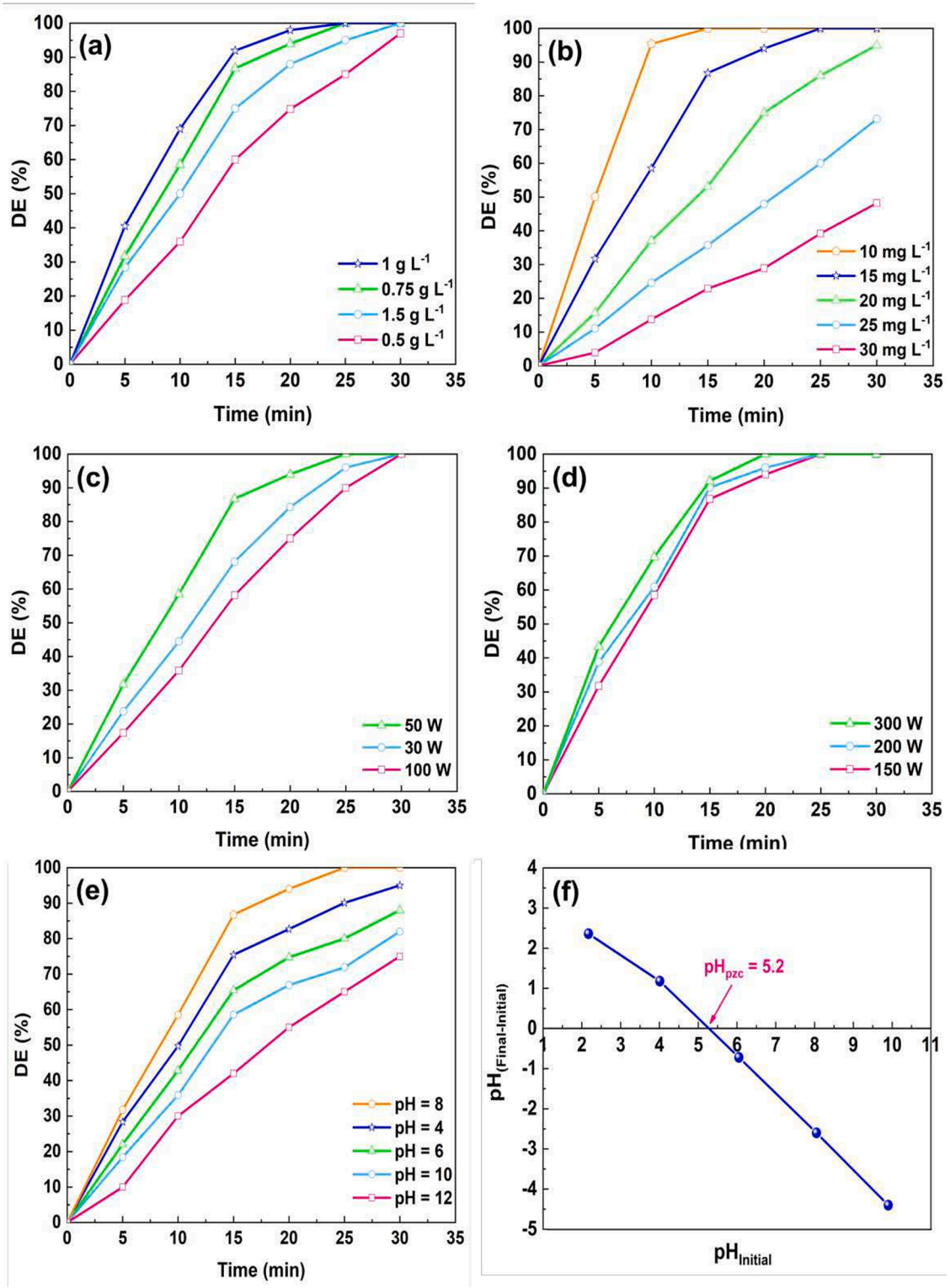

Fig. 4. The influence of (a) CuCr LDH/rGO concentration (b) DMP concentration, (c) visible light intensity, (d) US power, (e) pH, and (f) pH_{pzc} ($[DMP]_0 = 15$ mg L^{-1}, [CuCr LDH/rGO] = 0.75 g L^{-1}, pH = 8, US power = 150 W, and light intensity = 50 W).

unveiled that the highest DE% of 100% was achieved at pH = 8 (the natural pH of DMP) within 30 min of sonophotocatalysis. The obtained trend can be explained by employing the sonophotocatalyst's point of zero charges (pH_{pzc}). As shown in Fig. 4**f**, the pH_{pzc} of the CuCr LDH/rGO was calculated as 5.2. The surface of CuCr LDH/rGO is negatively charged at pH > 5.2 and positively charged at pH less than 5.2. Also, many influential parameters such as temperature, the amount of elemental content in catalyst structure, etc. can affect the functional groups and pH_{pzc}. As an instance, Siew et al. [38] reported that increasing the Fe^{2+} content in the catalyst framework decreased the pH_{pzc} to 4.0. They claimed that this decrease in pH_{pzc} is due to the increase in the number of free carboxylate groups remaining on the surface of the framework as a result of the increasing availability of free metal sites. Furthermore, Lalhmunsiama et al. [39] presented the

different amounts of pH_{pzc} for diverse graphene/graphene-based materials ranging from 4 to 10. Throughout the examination, DMP is in its nonionic form [40]. At pH less than 5.2, the CuCr LDH/rGO surface has a positive charge enhancing the attraction among an electron-rich aromatic ring or the oxygens of DMP and positive sites of the catalyst. Hence, the acidic condition is more beneficial than the basic condition due to the adsorption of more DMP molecules on the CuCr LDH/rGO surface. It was distinguished that higher adsorption amounts could boost photodegradation efficiency. Besides, in more basic conditions, the formed CO_2 during the DMP degradation process can be converted to CO_3^{2-}, consuming hydroxyl radical and resulting in a decrement in DE%. At pH = 8, the drawbacks that had been present at acidic and higher basic pHs diminished, and hydroxyl anions turned into hydroxyl radicals, increasing the rate of breakdown.

3.2.3. The retrievability of CuCr LDH/rGO

The performance of most nanocomposites is typically restricted by photo/sono corrosion over numerous experiments. Therefore, the stability of a nanocomposite is one of the most critical aspects for the wide application of the catalyst [8]. Considering this fact, the stability and reusability of the CuCr LDH/rGO were evaluated under 5 consecutive examinations. The results in Fig. S2**a** disclosed that the 15% decrement in the DE% occurred which is not significant after five cycles. This evidently demonstrated the capability of the CuCr LDH/rGO nanocomposite to disintegrate the target pollutants from the aqueous solution. Additionally, an assessment was performed on the nature of the recovered nanocomposite to identify the chemical and crystallographic alterations. As depicted in Fig. S2**b and c**, the FTIR and XRD patterns of the CuCr LDH/rGO resembled those of the fresh catalyst after five runs. This affirmed that there are no main structural changes in the CuCr LDH/rGO structure which can be utilized as a proper sonophotocatalyst.

3.2.4. The effect of scavengers and enhancers on sonophotocatalysis

With the aim of exploring the main active substances in the decomposition of DMP by CuCr LDH/rGO nanocomposite, a series of experiments were conducted in the presence of formic acid, p-benzoquinone, and isopropanol as h^+, $O_2^{\bullet-}$, and $^{\bullet}OH$ inhibitors, respectively. Fig. 5**a** represents the impact of diverse scavengers on the sonophotocatalytic activity of CuCr LDH/rGO. The DE% decreased from 100% in the absence of a scavenger to 92, 98, and 78 % in the existence of p-benzoquinone, formic acid, and isopropanol, respectively. Isopropanol demonstrated more declination in the DE% in comparison with p-benzoquinone and formic acid, which acknowledges the primary role of $^{\bullet}OH$ in the disintegration of DMP. It can be claimed that superoxide radicals and holes can participate in the degradation of DMP along with the hydroxyl radicals. Also, Daneshvar et al. [41] evaluated the impact of reactive species by the insertion of diverse quenchers. The obtained outcomes revealed that the hydroxyl radical is the dominant specie generated by ZnTi LDH during sonocatalysis [41]. To verify the involvement of hydroxyl radicals in degrading the pollutant, visual spectrophotometry with an O-phenylenediamine solution was conducted. As can be observed from Fig. 5**c**, the peak at 417 nm is attributed to the O-phenylenediamine-trapped $^{\bullet}OH$ radicals, which is enhanced by increasing the time of the sonophotocatalytic procedure.

The degradation of DMP in the presence of hydrogen peroxide (HP) and potassium peroxymonosulfate is represented in Fig. 5**b**. For this

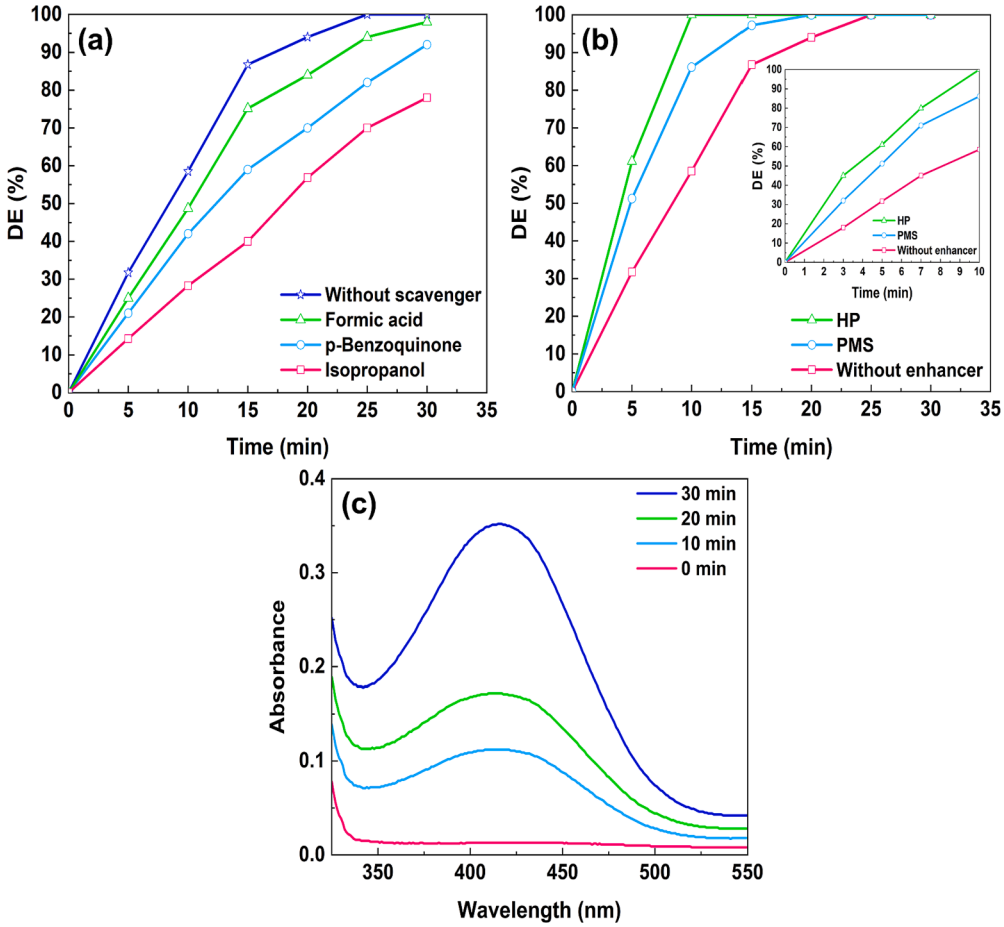

Fig. 5. The influence of (a) various scavengers, (b) enhancers on the DE% of DMP during sonophotocatalysis; inset demonstrates the effect of enhancers during 10 min of the treatment process ($[DMP]_0 = 15$ mg L^{-1}, [CuCr LDH/rGO] = 0.75 g L^{-1}, pH = 8, US power = 150 W, and light intensity = 50 W), and (c) the spectra of O-phenylenediamine-trapped hydroxyl radical.

experiment, oxidants with the concentration of 0.5 mmol L^{-1} were inserted into the DMP solution. During 10 min, the DE% of DMP was increased from 58.5% to 100% in the presence of HP. The generation of hydroxyl radicals is initiated by the reaction of H_2O_2 with Cu^{2+} and Cr^{3+} on the catalyst surface (**Eqs. (1–3)**), where M^{n+} is Cu^{2+} or Cr^{3+} and M^{n+1} is their redox pairs. Also, the achieved improvement can be related to the formation of hydroxyl radicals from HP under US and light irradiations (**Eq. (4)**).

$$M^{n+} + H_2O_2 \rightarrow M^{n+1} + OH^{\bullet} + OH^{-} \quad (1)$$

$$M^{n+1} + H_2O_2 \rightarrow H^{+} + M\text{-}OOH^{n+} \quad (2)$$

$$M\text{-}OOH^{n+} \rightarrow HO_2^{\bullet} + M^{n+} \quad (3)$$

$$H_2O_2 \xrightarrow{US/hE} 2OH^{\cdot} \quad (4)$$

With the addition of PMS to the reaction media, the DE% improved from 58.5% to 86% during 10 min. The pathway of PMS activation in the presence of CuCr LDH is shown in **Eqs. (5) and (6)** [42]. Sulfate radicals can be generated by the reaction of PMS with the surface OH functional groups of the catalyst [43]. Furthermore, PMS can be reacted with the electron and holes aroused from the sonophotocatalytic process to produce further amounts of ROSs (**Eqs. 7–9**) [26].

$$M\text{-}OH + HSO_5^{-} \rightarrow M\text{-}(O)OSO_3^{-} + H_2O \quad (5)$$

$$2M\text{-}(O)OSO_3^{-} + 2H_2O \rightarrow 2M\text{-}OH^{-} + O_2 + 2SO_4^{\bullet -} + 2H^{+} \quad (6)$$

$$HSO_5^{-} + e^{-} \rightarrow OH^{\bullet} + SO_4^{2-} \quad (7)$$

$$HSO_5^{-} + h^{+} \rightarrow H^{+} + SO_5^{\bullet -} \quad (8)$$

$$2SO_5^{\bullet -} \rightarrow O_2 + 2SO_4^{\bullet -} \quad (9)$$

3.3. The produced by-products and degradation mechanism

The generated intermediates of the DMP degradation under the sonophotocatalytic process at the optimized condition were identified by GC–MS analysis. As manifested in **Table S1**, during the reaction time, four by-products with retention times of 5.54, 13.86, 24.62, and 24.99 min appeared. Initially, the hydrolyzation of the side ester group of DMP occurred through the attack of the predominated ROSs, according to the GC–MS outcomes. The same process was reported previously by Yegane Badi et al. [44]. Afterward, the aromatic ring of DMP and intermediate products were cleaved to yield alkanes. Further oxidations can generate simple-structured aldehydes and acids which would ultimately undergo mineralization to form water and carbon dioxide. This must be acknowledged that owing to the rapid oxidation, additional intermediates may be obtained that were not identified.

4. Conclusion

To sum up, CuCr LDH and its graphene-based nanocomposites were synthesized via eco-friendly and sustainable techniques, which were then employed as novel sonophotocatalysts for DMP degradation. The order of DE% through sonophotocatalysis in the presence of the so-synthesized catalysts is CuCr LDH (42%) < CuCr LDH/GO (58.5%) < CuCr LDH/rGO (100%), which is related to the several features including a narrow bandgap and high specific surface area, as validated by DRS and BET analyses, respectively. Under simultaneous irradiations of 150 W US and 50 W light, 0.75 g L^{-1} of CuCr LDH/rGO exhibits a high DE% of 100% during 30 min in the original pH of DMP with a concentration of 15 mg L^{-1}. Meanwhile, hydroxyl radical plays a prominent role in the disintegration of DMP through sonophotocatalysis. The reusability of the CuCr LDH/rGO was evaluated after 5 consecutive runs. The 15% reduction of DE% and physical/chemical stability of the CuCr LDH/rGO after 5 runs can introduce it as a robust catalyst. Lastly, According to the EEO value calculations, sonophotocatalytic decomposition of DMP by CuCr LDH/rGO can be regarded as a cost-effective route for the decomposition of recalcitrant contaminants in comparison with similar findings.

CRediT authorship contribution statement

Tannaz Sadeghi Rad: Writing – original draft, Methodology, Data curation, Software. **Emine Sevval Yazici:** Formal analysis, Data curation. **Alireza Khataee:** Supervision, Project administration, Writing – review & editing, Resources. **Erhan Gengec:** Funding acquisition, Resources, Writing – review & editing. **Mehmet Kobya:** Conceptualization, Investigation, Resources.

Declaration of Competing Interest

The authors declare that they have no known competing financial interests or personal relationships that could have appeared to influence the work reported in this paper.

Data availability

No data was used for the research described in the article.

Acknowledgment

The authors are appreciative of the support supplied by the Scientific and Technical Research Council of Turkey (TUBITAK, Project number of 120Y350).

Appendix A. Supplementary data

Supplementary data to this article can be found online at https://doi.org/10.1016/j.ultsonch.2023.106358.

References

[1] S. Ding, J. Wan, Y. Wang, Z. Yan, Y. Ma, Activation of persulfate by molecularly imprinted Fe-MOF-74@SiO_2 for the targeted degradation of dimethyl phthalate: Effects of operating parameters and chlorine, Chem. Eng. J. 422 (2021), 130406, https://doi.org/10.1016/j.cej.2021.130406.

[2] S. Net, R. Sempéré, A. Delmont, A. Paluselli, B. Ouddane, Occurrence, fate, behavior and ecotoxicological state of phthalates in different environmental matrices, Environ. Sci. Technol. 49 (2015) 4019–4035, https://doi.org/10.1021/es505233b.

[3] Y. Hu, Q. Niu, Y. Wang, Y. Zhang, G. Zhao, Highly efficient removal mechanism of dimethyl phthalate over an economical 3D {001}TiO_2/Ti photoelectrode with enhanced photoelectrocatalytic activity and long service life, Appl. Catal. B Environ. 285 (2021), 119812, https://doi.org/10.1016/j.apcatb.2020.119812.

[4] A. Paluselli, V. Fauvelle, F. Galgani, R. Sempéré, Phthalate release from plastic fragments and degradation in seawater, Environ. Sci. Technol. 53 (2019) 166–175, https://doi.org/10.1021/acs.est.8b05083.

[5] V.K. Sharma, M. Feng, Water depollution using metal-organic frameworks-catalyzed advanced oxidation processes: A review, J. Hazard. Mater. 372 (2019) 3–16, https://doi.org/10.1016/j.jhazmat.2017.09.043.

[6] S. Moradi, C. Rodriguez-Seco, F. Hayati, D. Ma, Sonophotocatalysis with photoactive nanomaterials for wastewater treatment and bacteria disinfection, ACS Nanosci. Au. (2023), https://doi.org/10.1021/acsnanoscienceau.2c00058.

[7] A. Rey, J. Carbajo, C. Adán, M. Faraldos, A. Bahamonde, J.A. Casas, J.J. Rodriguez, Improved mineralization by combined advanced oxidation processes, Chem. Eng. J. 174 (2011) 134–142, https://doi.org/10.1016/j.cej.2011.08.061.

[8] A. Khataee, T.S. Rad, S. Nikzat, A. Hassani, M.H. Aslan, M. Kobya, E. Demirbaş, Fabrication of NiFe layered double hydroxide/reduced graphene oxide (NiFe-LDH/rGO) nanocomposite with enhanced sonophotocatalytic activity for the degradation of moxifloxacin, Chem. Eng. J. 375 (2019), 122102, https://doi.org/10.1016/j.cej.2019.122102.

[9] J. Theerthagiri, S.J. Lee, K. Karuppasamy, S. Arulmani, S. Veeralakshmi, M. Ashokkumar, M.Y. Choi, Application of advanced materials in sonophotocatalytic processes for the remediation of environmental pollutants, J. Hazard. Mater. 412 (2021), 125245, https://doi.org/10.1016/j.jhazmat.2021.125245.

[10] T.S. Rad, Z. Ansarian, R.D.C. Soltani, A. Khataee, Y. Orooji, F. Vafaei, Sonophotocatalytic activities of FeCuMg and CrCuMg LDHs: Influencing factors,

antibacterial effects, and intermediate determination, J. Hazard. Mater. 399 (2020), 123062, https://doi.org/10.1016/j.jhazmat.2020.123062.
[11] A. Hameed, M. Batool, Z. Liu, M.A. Nadeem, R. Jin, Layered double hydroxide-derived nanomaterials for efficient electrocatalytic water splitting: Recent progress and future perspective, ACS Energy Lett. 7 (2022) 3311–3328, https://doi.org/10.1021/acsenergylett.2c01362.
[12] H. Li, C. Mao, H. Shang, Z. Yang, Z. Ai, L. Zhang, New opportunities for efficient N_2 fixation by nanosheet photocatalysts, Nanoscale. 10 (2018) 15429–15435, https://doi.org/10.1039/C8NR04277B.
[13] Y. Zhao, X. Jia, G.I.N. Waterhouse, L.-Z. Wu, C.-H. Tung, D. O'Hare, T. Zhang, Layered double hydroxide nanostructured photocatalysts for renewable energy production, Adv. Energy Mater. 6 (2016) 1501974, https://doi.org/10.1002/aenm.201501974.
[14] T. Sadeghi Rad, E.S. Yazici, A. khataee, E. Gengec, M. Kobya, Nanoarchitecture of graphene nanosheets decorated with NiCr layered double hydroxide for sonophotocatalytic degradation of refractory antibiotics, Environ. Res. 214 (2022) 113788.
[15] Z. Huang, P. Wu, Y. Lu, X. Wang, N. Zhu, Z. Dang, Enhancement of photocatalytic degradation of dimethyl phthalate with nano-TiO_2 immobilized onto hydrophobic layered double hydroxides: A mechanism study, J. Hazard. Mater. 246–247 (2013) 70–78, https://doi.org/10.1016/j.jhazmat.2012.12.016.
[16] Q. Ye, J. Wu, P. Wu, S. Rehman, Z. Ahmed, N. Zhu, Enhancing peroxymonosulfate activation by Co-Fe layered double hydroxide catalysts via compositing with biochar, Chem. Eng. J. 417 (2021), 129111, https://doi.org/10.1016/j.cej.2021.129111.
[17] M. Li, B. Yin, C. Gao, J. Guo, C. Zhao, C. Jia, X. Guo, Graphene: Preparation, tailoring, and modification, Exploration. 3 (2023) 20210233, https://doi.org/10.1002/EXP.20210233.
[18] M.A. Ahmed, A.A. Mohamed, Recent progress in semiconductor/graphene photocatalysts: synthesis, photocatalytic applications, and challenges, RSC Adv. 13 (2023) 421–439, https://doi.org/10.1039/D2RA07225D.
[19] Y.F. Fang, A.P. Deng, Y.P. Huang, Determination of hydroxyl radical in Fenton system, Chin. Chem. Lett. 20 (2009) 1235–1240, https://doi.org/10.1016/j.cclet.2009.05.004.
[20] A.S. Patil, J.L. Gunjakar, C.D. Lokhande, U.M. Patil, S.V. Sadavar, N.S. Padalkar, R. B. Shinde, M.M. Wagh, J.S. Bagi, Nanocrystalline copper-chromium-layered double hydroxide with tunable interlayer anions for electrochemical capacitor application, Synth. Met. 264 (2020), 116371, https://doi.org/10.1016/j.synthmet.2020.116371.
[21] S. Ziegenheim, G. Varga, M. Szabados, P. Sipos, I. Pálinkó, Cu(II)Cr(III)-LDH: synthesis, characterization, intercalation properties and a catalytic application, Chem. Pap. 72 (2018) 897–902, https://doi.org/10.1007/s11696-017-0352-z.
[22] D.P. Sahoo, S. Patnaik, D. Rath, K. Parida, Synergistic effects of plasmon induced Ag@ Ag_3VO_4/ZnCr LDH ternary heterostructures towards visible light responsive O_2 evolution and phenol oxidation reactions, Inorg. Chem. Front. 5 (2018) 879–896, https://doi.org/10.1039/C7QI00742F.
[23] H. Abdolmohammad-Zadeh, K. Nejati, E. Ghorbani, Synthesis, characterization, and application of Zn–Al layered double hydroxide as a nano-sorbent for the removal of direct Red 16 from industrial wastewater effluents, Chem. Eng. Commun. 202 (2015) 1349–1359, https://doi.org/10.1080/00986445.2014.927357.
[24] S.S. Ravuru, A. Jana, S. De, Synthesis of NiAl- layered double hydroxide with nitrate intercalation: Application in cyanide removal from steel industry effluent, J. Hazard. Mater. 373 (2019) 791–800, https://doi.org/10.1016/j.jhazmat.2019.03.122.
[25] T. Sadeghi Rad, A. Khataee, S. Arefi-Oskoui, S. Sadeghi Rad, Y. Orooji, E. Gengec, M. Kobya, Graphene-based ZnCr layered double hydroxide nanocomposites as bactericidal agents with high sonophotocatalytic performances for degradation of rifampicin, Chemosphere. 286 (2022) 131740.
[26] A. Fazli, M. Brigante, A. Khataee, G. Mailhot, Synthesis of a magnetically separable LDH-based S-scheme nano-heterojunction for the activation of peroxymonosulfate towards the efficient visible-light photodegradation of diethyl phthalate, Appl. Surf. Sci. 559 (2021), 149906, https://doi.org/10.1016/j.apsusc.2021.149906.
[27] K.S.W. Sing, Reporting physisorption data for gas/solid systems with special reference to the determination of surface area and porosity (Recommendations 1984), Pure Appl. Chem. 57 (1985) 603–619. Doi: 10.1351/pac198557040603.
[28] Y. Zhang, C. Jing, J. Zheng, H. Yu, Q. Chen, L. Guo, D. Pan, N. Naik, Q. Shao, Z. Guo, Microwave hydrothermal fabrication of CuFeCr ternary layered double hydroxides with excellent Cr(VI) adsorption, Colloids Surf. Physicochem. Eng. Asp. 628 (2021), 127279, https://doi.org/10.1016/j.colsurfa.2021.127279.
[29] M. Roso, C. Boaretti, M.G. Pelizzo, A. Lauria, M. Modesti, A. Lorenzetti, Nanostructured photocatalysts based on different oxidized graphenes for VOCs removal, Ind. Eng. Chem. Res. 56 (2017) 9980–9992, https://doi.org/10.1021/acs.iecr.7b02526.
[30] F. Rahmani, A. Ghadi, E. Doustkhah, S. Khaksar, In situ formation of copper phosphate on hydroxyapatite for wastewater treatment, Nanomaterials. 12 (2022) 2650, https://doi.org/10.3390/nano12152650.
[31] R. Patidar, V.C. Srivastava, Mechanistic and kinetic insights of synergistic mineralization of ofloxacin using a sono-photo hybrid process, Chem. Eng. J. 403 (2021), 125736, https://doi.org/10.1016/j.cej.2020.125736.
[32] G. Fan, X. Lin, S. Yang, B. Du, Y. Lu, X. Huang, J. Wu, K.-Q. Xu, Design of continuous flow membrane reactor for in-situ sonophotocatalytic degradation of ciprofloxacin, J. Environ. Chem. Eng. 10 (6) (2022) 108888.
[33] E. Dikmen, G. Dogdu, A. Yalcuk, Comparison performances of hybrid sonocatalysis and sonophotocatalysis on the elimination of 2,4-dichlorophenoxyacetic acid in water: Mineralization and economic analysis, Pol. J. Environ. Stud. 31 (2022) 4589–4602. https://doi.org/10.15244/pjoes/149575.
[34] X. Zhang, X. Wang, J. Chai, S. Xue, R. Wang, L. Jiang, J. Wang, Z. Zhang, D. D. Dionysiou, Construction of novel symmetric double Z-scheme $BiFeO_3$/$CuBi_2O_4$/$BaTiO_3$ photocatalyst with enhanced solar-light-driven photocatalytic performance for degradation of norfloxacin, Appl. Catal. B Environ. 272 (2020), 119017, https://doi.org/10.1016/j.apcatb.2020.119017.
[35] A.A. Oladipo, A.O. Ifebajo, M. Gazi, Magnetic LDH-based CoO–$NiFe_2O_4$ catalyst with enhanced performance and recyclability for efficient decolorization of azo dye via Fenton-like reactions, Appl. Catal. B Environ. 243 (2019) 243–252, https://doi.org/10.1016/j.apcatb.2018.10.050.
[36] N. Askari, M. Beheshti, D. Mowla, M. Farhadian, Facile construction of novel Z-scheme $MnWO_4$/Bi_2S_3 heterojunction with enhanced photocatalytic degradation of antibiotics, Mater. Sci. Semicond. Process. 127 (2021), 105723, https://doi.org/10.1016/j.mssp.2021.105723.
[37] L. Xu, N.-P. Liu, H.-L. An, W.-T. Ju, B. Liu, X.-F. Wang, X. Wang, Preparation of Ag_3PO_4/$CoWO_4$ S-scheme heterojunction and study on sonocatalytic degradation of tetracycline, Ultrason. Sonochem. 89 (2022), 106147, https://doi.org/10.1016/j.ultsonch.2022.106147.
[38] W.Y. Siew, N.H.H. Abu Bakar, M. Abu Bakar, A. Zainal Abidin, Influence of various Cu/Fe ratios on the surface properties of green synthesized Cu-Fe-BTC and it's relation to methylene blue adsorption, J. Hazard. Mater. 416 (2021), 125846, https://doi.org/10.1016/j.jhazmat.2021.125846.
[39] L. Lalhmunsiama, N. Ngainunsiami, D.-J. Kim, D. Tiwari, Graphene based advanced materials in the remediation of aquatic environment contaminated with fluoride: Newer insights and applicability, Chem. Eng. Process. - Process Intensif. 165 (2021), 108428, https://doi.org/10.1016/j.cep.2021.108428.
[40] G. Wang, Q. Chen, Y. Liu, D. Ma, Y. Xin, X. Ma, X. Zhang, In situ synthesis of graphene/WO_3 co-decorated TiO_2 nanotube array photoelectrodes with enhanced photocatalytic activity and degradation mechanism for dimethyl phthalate, Chem. Eng. J. 337 (2018) 322–332, https://doi.org/10.1016/j.cej.2017.12.058.
[41] H. Daneshvar, M.S. Seyed Dorraji, A.R. Amani-Ghadim, M.H. Rasoulifard, Enhanced sonocatalytic performance of ZnTi nano-layered double hydroxide by substitution of Cu (II) cations, Ultrason. Sonochem. 58 (2019), 104632, https://doi.org/10.1016/j.ultsonch.2019.104632.
[42] T. Zhang, H. Zhu, J.-P. Croué, Production of sulfate radical from peroxymonosulfate induced by a magnetically separable $CuFe_2O_4$ spinel in water: Efficiency, stability, and mechanism, Environ. Sci. Technol. 47 (2013) 2784–2791, https://doi.org/10.1021/es304721g.
[43] X. Zheng, X. Niu, D. Zhang, M. Lv, X. Ye, J. Ma, Z. Lin, M. Fu, Metal-based catalysts for persulfate and peroxymonosulfate activation in heterogeneous ways: A review, Chem. Eng. J. 429 (2022), 132323, https://doi.org/10.1016/j.cej.2021.132323.
[44] M.Y. Badi, A. Esrafili, H. Pasalari, R.R. Kalantary, E. Ahmadi, M. Gholami, A. Azari, Degradation of dimethyl phthalate using persulfate activated by UV and ferrous ions: optimizing operational parameters mechanism and pathway, J. Environ. Health Sci. Eng. 17 (2019) 685–700, https://doi.org/10.1007/s40201-019-00384-9.